Journal of Neurochemistry, 2006, **99**, 537–548 doi:10.1111/j.1471-4159.2006.04072.x

Hierarchy and the mechanism of fibril formation in ADan peptides

Ira Surolia,* G. Bhanuprakash Reddy* and Sharmistha Sinha†

**National Institute of Nutrition, Hyderabad, India*

†*Molecular Biophysics Unit, Indian Institute of Science, Bangalore, India*

Abstract

Familial Danish dementia is a neurodegenerative disease which is a consequence of alterations in the *BRI* gene. The pathological signatures of the disease are cerebral amyloidolysis, parenchymal protein deposits and neuronal degeneration. Synthetic Danish dementia (ADan) peptides are capable of forming fibrillar assemblies *in vitro* at pH 4.8. However, the morphology of the aggregates formed depends greatly on the form of the peptides (oxidized or reduced). In addition to long slender assemblies (2–5 nm in diameter and several micrometers in length) we report ring-like or annular masses (8–9 nm in diameter and 1–2 mm in perimeter) in the case of the oxidized form of the peptides. The reduced forms mainly aggregate to produce granular heaps. The biophysical and kinetic characterization of the process of aggregation was carried out using different spectroscopic and imaging techniques. Neurotoxicity assays performed on both the forms reveal that the toxicity bears proportionality with the aggregate size.

Keywords: amyloids, annular aggregation, Danish dementia, fibrils, protein aggregation.

J. Neurochem. (2006) **99**, 537–548.

A number of proteins follow uncustomary folding and adopt incorrect folds different from their native forms (Ramos and Ferreira 2005). In time, these structures are either ubiquitinated or form insoluble deposits, like those of amyloid fibrils, which are the hallmark of most neurodegenerative diseases (Horwich and Weissman 1997; Dobson 1999; Soto 2003; Agorogiannis *et al*. 2004; Foguel and Silva 2004; Ross and Pickart 2004). Normally, these deposits are β-pleated sheets with distinct morphological features and, once formed, mostly remain unperturbed. The literature has examples of an ample number of proteins that have a tendency to form amyloid plaques and are associated with specific human diseases such as Alzheimer's disease, Parkinson's disease, Huntington's disease, etc. (Selkoe 2004; Thompson and Barrow 2002; Recchia *et al*. 2004). To date, a repertoire of 25 human proteins has been documented to form amyloid fibrils, and several factors can influence their formation (Westernmark 2005; Mitra *et al*. 2006). Most of the amyloid deposits have been shown to be neurotoxic to cells in culture and are considered to be the cause for the neurodegenertion and neuronal apathy. Investigators in this field have tried to evaluate the nature of these deposits by working on small peptide fragments (which are the part of the full-length protein that contribute essentially to the process of fibrillation) rather than working on the full-length protein. These short peptides, either synthesized or expressed, give a wealth of information about the organization of these assemblies. For example, recently, Nelson *et al*. (2005) have shown the cross β-spine architecture of the GNNQQNY and NNQQNY peptides using X-ray crystallography . Similarly, a recent report on a modelled dipeptide (Leu-Cys/Val-Cys) demonstrates the role of disulfide bonds on the fate of these fibres (Das *et al*. 2005). Other synthetic short peptides involved in elucidating the physical aspects of these fibres include NFGAIL (a portion of the islet amyloid polypeptide), AGAAAAGA (the amyloidogenic region in prion proteins) and polyglutamine peptide D2Q15K2 (Ma and Nussinov 2002; Zanuy *et al*. 2003; Sikorski and Atkins 2005). A general structural element that has resulted from these studies (modelling, simulations or spectroscopic) is that these share a common kind of design of a β-sheet accumulation which is

Received March 18, 2006; revised manuscript received June 7, 2006; accepted June 7, 2006.

Address correspondence and reprint requests to Sharmistha Sinha, Molecular Biophysics Unit, Indian Institute of Science, Bangalore-560012, India. E-mail: sinhas@mbu.iisc.ernet.in

Abbreviations used: ADan, Danish dementia; AFM, atomic force microscopy; CD, circular dichroism; MTT, 3-(4,5-dimethylthiazol-2-yl)-2,5-diphenyltetrazolium bromide; oxAdan, oxidized peptide; redAdan, reduced peptides; SDS–PAGE, sodium dodecyl sulfate – polyacrylamide gel electrophoresis; TEM, transmission electron microscopy; ThT, Thioflavin-T; UV, ultraviolet.

stabilized by hydrogen bonding, ionic interactions, π–π stacking of the aromatic groups and hydrophobic interactions.

The formation of these fibrillar deposits may thus be defined as a 'self-assembly' process in which small peptides containing suitable conformations combine to form a supra molecular β-sheet kind of architecture. These fibres show a distinctive interaction with hetero-aromatic dyes and the spectroscopic responses as a result of these interactions are very explicit. The deposits are characterized as fibres of 4–10 nm in diameter which exhibit red–green birefringes under crossed polarized light when stained with Congo red dye, and a yellow–green luminescence with Thioflavin-T (ThT; Pras *et al*. 1968; Krebs *et al*. 2004).

Familial Danish dementia is a neurodegenerative disorder linked to a genetic defect in the *BRI2* gene. It is typified by deafness, cataracts, ataxia and dementia. Histological signatures of the disease are cerebral amyloid angiopathy, parenchymal protein deposits and neurofibrillary degeneration which are analogous to those in Alzheimer's disease (Vidal *et al*. 2000). The Danish dementia (ADan) peptide is a 34-amino acid-long peptide which is thought to be the major cause of amyloid deposition in brains of patients suffering from familial Danish dementia. This study focuses on the kinetics and morphological features of the filamentous structures formed from the 4-kDa ADan peptide. Similar studies carried out on ABri peptides reveal that the fibres formed have an average size of 3–4 nm (Srinivasan *et al*. 2003). The authors report a pH-dependent aggregation of the peptides and a hierarchical mechanism of amyloid plaque formation in ABri peptides. While they originate from different genetic defects in the *BRI* gene, ADan and ABri peptides have a number of common features. The amyloid precursor proteins in the British family (ABriPP) and in the Danish family (ADanPP) have the same length of 277 amino acids. Also, ABri and ADan peptides have the same sequence length and share identical N-terminal amino acid sequence (the first 22 residues), which suggests that these molecules are generated by the same proteolytic mechanism (Vidal *et al*. 2000). Earlier reports on ADan peptides have shown that both the oxidized (Cys4 and Cys21 are linked by an intramolecular disulfide bond) and the reduced (no intramolecular disulfide bond present) form of the peptide is incompetent in producing fibres at pH 7.0 (Gibson *et al*. 2004). We also report that the toxicity of the reduced form is greater than that of the oxidized form. Our studies demonstrate that, while the oxidized peptide (oxADan) is the dominant fibre-forming entity at pH 4.8, the reduced form is not capable of doing so at any pH, and a wide range of concentrations and toxicity depends on the size of the aggregates rather than on the form. Further, we demonstrate a cascade mechanism of fibre formation in the oxADan peptides.

Materials and methods

Preparation of ADan peptide solutions

The reduced and the oxidized form of ADan peptides and Aβ-40 peptides were bought from Bachem (Torrance, CA, USA) and purified using a C-18 HPLC column in a WATERS HPLC (Milford, MA, USA). The purity and mass of the peptides were assessed by MALDI-TOF mass spectrometry (Bruker Daltonics, Bremen, Germany; Fig. 1). The peptides were further purified using HPLC and the mass was detected using MALDI. All the studies were carried out in the peptide concentration range of 3–200 μM. The peptides were subjected to a 1,1,1,3,3,3-hexafluoro-2-propanol (HFIP) treatment (see Stine *et al*. 2003) with a slight modification.

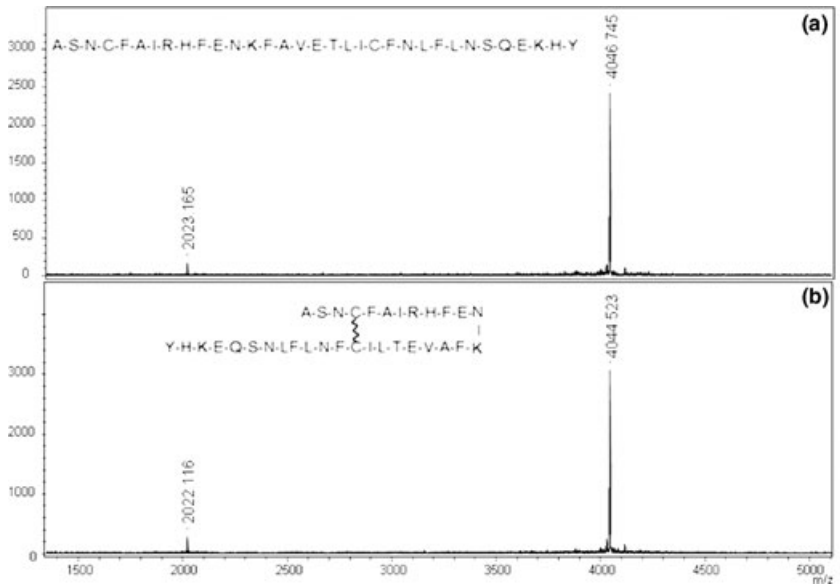

Fig. 1 The MALDI mass spectrum of HPLC-purified ADan peptides; (a) redADan and (b) oxADan peptides. The primary sequence of the respective peptides is shown on each mass spectrum.

Briefly, the peptides were dissolved in 1,1,1,3,3,3-hexafluoro-2-propanol and sonicated in a water bath for 1 h, followed by vortexing for 15 min. This solution was left in 1,1,1,3,3,3-hexafluoro-2-propanol overnight. The solution was lyophilized and then taken for fibrilization. The lyophilized peptides obtained were dissolved in a minimum volume of dimethylsulfoxide (DMSO) under a flow of liquid nitrogen. This became the stock solution. In this way, peptides can be stored in DMSO for a period of almost a month without any aggregation. From this stock solution, peptide solutions of 3, 9, 18, 35, 70, 100 and 140 μM were prepared at pH 4.8 (5 mM sodium acetate buffer, 10 μM sodium chloride and 0.03% sodium azide) and kept for oligomerization. Similarly, solutions containing 70 μM peptide were made at pH 6 (10 mM HEPES buffer, 10 mM sodium chloride and 0.03% sodium azide), 7.4 and 8.5 (phosphate buffer, 10 mM sodium chloride and 0.03% sodium azide). These solutions were used in the studies described below. Stocks of Aβ peptides were also made in DMSO and kept for control studies. Of the peptide solutions, 40 μM were employed for further studies.

Thioflavin-T assays

The ThT binding assays were performed as described by Nielsen *et al*. (2001), with slight modification. Briefly, the ADan and the Aβ peptides were excited at 444 nm and emission was taken in the range of 460–560 nm (in a Jobin Yvon Fluoromax spectrofluorometer (Jobin Yvon (Spex division), Cedex, France) using an excitation slit width of 2 nm and emission of 5 nm) at the respective pHs and at the range of concentrations mentioned above. Prior to each fluorescence measurement, 10 μL of 100 μM of ThT was incubated with 110 μL of the ADan peptides for 30 min. These assays were performed with the Aβ peptides at a concentration of 40 μM and a pH of 2.0, 4.8 and 8.0.

Congo red binding and birefringes

Aliquots (20 μL) of 1.25 mM ADan and Aβ peptides, aged for 1 month, were added to 100 μL of 1 mM Congo red solution at pH 4.8. This solution was incubated for an hour at room temperature (25°C) and centrifuged. The resulting pellet was kept on a slide covered by a coverslip and observed under a crossed polarized light (Pras *et al*. 1968).

Fluorescence polarization experiments

The polarization experiments for the single tyrosine residue at the C-terminal were performed in a Jobin Yvon Fluorolog spectrofluorometer using an excitation slit width of 2 nm and emission of 5 nm at pH 4.8. The oxADan oxidized peptides samples were excited at 280 nm and polarization was recorded at 305 nm. The peptide concentration used was 100 μM. For the centrifuged samples, solutions were centrifuged at 12577.5 *g* for 30 min and the supernatant was taken for polarization measurements. The polarization was calculated according to the equation $P = (I_{\|} - I_{\perp})/(I_{\|} + I_{\perp})$, where $I_{\|}$ is the fluorescence in the parallel direction and $I_{\perp}$ is the fluorescence in the perpendicular direction.

Size exclusion chromatography

At various time points, aliquots of the 200 μM ADan peptides incubated at pH 4.8 (sodium acetate buffer 5 μM, 10 mM sodium chloride and 0.03% sodium azide) were loaded on to a Superdex-75 (Sigma-Aldrich, St. Louis, MO, USA) gel filtration column (10 × 110 mm) in 5 mM Na-actetate buffer at pH 4.8. The elute was monitored at 215 nm.

Transmission electron microscopy (TEM)

Aged ADan and Aβ peptides were centrifuged for 10 min at 5590 *g* and then the pellet was re-suspended in 20 μL of the supernatant. This suspension was then loaded on to a 300-mesh carbon-coated copper grid. The samples were then negatively stained by 2% uranyl acetate for 2 min followed by drying the grids under an infrared lamp for 10 min. The grids were then visualized using an acceleration voltage of 120 kV in a Fei Tecnai $G^2$12 (Eindhoven, The Netherlands) cryo-electron microscope (Ruben *et al*. 1993).

Gel electrophoresis

The aggregation of the ADan peptides was determined by sodium dodecyl sulfate – polyacrylamide gel electrophoresis (SDS–PAGE) on 15% gels. The lyophilized peptides were dissolved in 5 mM Na-acetate buffer at pH 4.8 at a concentration of 0.4 mg/mL. These solutions were then incubated at 25°C for a period of 12–15 days. Aliquots of 50 μL were drawn out at different time points and immediately dried in a speedvac concentrator. These dried samples were then stored at −20°C until analysis. The samples were dissolved in 40 μL of SDS loading buffer prior to electrophoresis. The peptides were visualized on the gel by silver staining (Laemmli 1970).

Circular dichroism

Circular dichroism (CD) studies were performed in a Jasco-J715 polarimeter (Jasco Corporation, Tokyo, Japan) in a 0.01-cm path-length cell for far ultraviolet (UV)–CD with a slit width of 1 nm, response time of 4 s and scan speed of 50 nm/s. Each scan was an average of 32 scans (Srinivasan *et al*. 2003).

Atomic force microscopy (AFM)

A drop of aged ADan or Aβ peptide solution was placed on a freshly cleaved mica sheet and immediately dried under nitrogen gas. The salt deposits were washed extensively with miliQ (Milipore, Champigneulles, France) water. The samples were once again dried with nitrogen gas. All the images were recorded in air under ambient conditions with a scan rate of 0.3 Hz in a WITec (Horvelsinger Weg6, Germany) AFM instrument. The resonance frequency used was 75 kHz (Ionescu-Zanetti *et al*. 1999).

Cell neurotoxicity assay

3-(4,5-Dimethylthiazol-2-yl)-2,5-diphenyltetrazolium bromide (MTT) assay

The effect of ADan peptides on cell viability was assessed by measuring residual cellular redox activity with an MTT assay (Sigma, St Louis, MO, USA) as previously described (Gibson *et al*. 2004). Briefly, cells (in RPMI medium with 5% fetal bovine serum) were plated at 10^5 cells/well in 96-well plates in 90 μL of fresh medium. Prior to this, the peptides were aged at 25°C for 4–5 days (in 5 mM sodium acetate buffer containing 10 mM sodium chloride), lyophilized and kept at −20°C in a nitrogen atmosphere. The peptides were then re-suspended in fresh medium and added to the cells in the plate. Cells were then incubated at 37°C in 5% CO_2 for

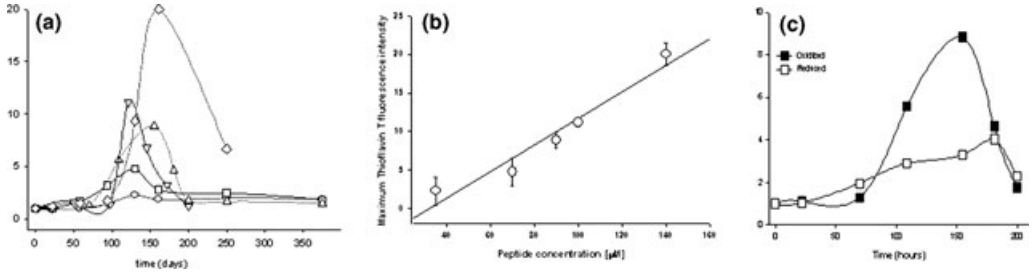

Fig. 2 Thioflavin-T fluorescence compared for its interaction with the oxADan and redADan peptides. The samples were excited at 444 nm and the emission was collected at 482 nm. (a) The oxADan peptide concentrations used are 18 μM (○), 35 μM (□), 70 μM (▽), 100 μM (△) and 140 μM (◇). (b) Maximum Thioflavin-T intensity attained by the fibres formed from different oxADan peptide concentrations. (c) Comparing the aggregation kinetics of the reduced (□) and the oxidized (■) form by Thioflavin-T fluorescence. The peptide concentration used was 100 μM.

24 h, following which MTT was added to a final concentration of 0.5 mg/mL and the plates were incubated at 37°C for 3 h. The formazan formed was solubilized in isopropyl alcohol (150 μL) and incubated overnight at 37°C. Finally, the absorbance values at 570 nm were measured.

Trypan blue exclusion assay

The cell viability was also tested by trypan blue exclusion assay. Viability assays measure the percentage of a cell mass that is viable. This is generally accomplished by a dye exclusion stain, where cells with an intact membrane are able to exclude the dye while cells without an intact membrane take up the colouring agent. Neuro2a cells (10^6 cells/well) were incubated with the desired concentration of the fibres for 24 h at 37°C in 5% CO_2. A 0.4% trypan blue solution was added to each well and incubated for 2 min. Cells were counted using a heamocytometer. The calculated percentage of unstained cells represented the percentage of viable cells (Phillips 1973).

Results

Fibrillogenesis – reduced peptides (redADan) versus oxADan

The ThT assays, Congo red birefringes and AFM/TEM imaging clearly indicated that only the oxidized form of the peptides are capable of integrating themselves into fibrillar assemblies, while the reduced form can only assemble to form globular objects of a defined topology. The ThT assays, when compared for the two forms, illustrated that the enhancement in the fluorescence signal for the oxidized form is much more than that of the reduced one (Fig. 2), thus validating the capability of the oxADan to form fibres over the redADan. The implications from the imaging studies and CD experiments were similar (Fig. 3). Figures 4–7 show the nature of aggregates formed from the oxADan and redADan peptides as visualized by AFM and TEM. A brief description of the morphology of the aggregates is discussed in a latter section. Strong red–green birefringes with Congo red dye were observed for the oxidized peptides alone (Fig. 7e) and not for the reduced ones (data not shown).

Fibrillogenesis – Aβ versus oxADan

Figure 8 shows the entire event of fibril formation in Aβ peptides (used here as the positive control) as monitored by

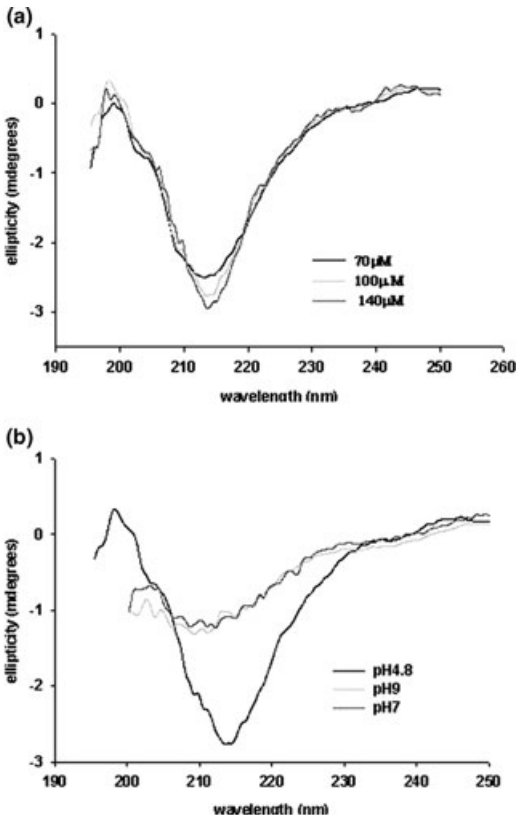

Fig. 3 Far UV circular dichroism spectra of oxADan peptides. Peptide solutions were incubated for 5 days at (a) pH 4.8 at different peptide concentrations as indicated and at (b) 140-μM peptide concentrations in buffers of different pH values as indicated.

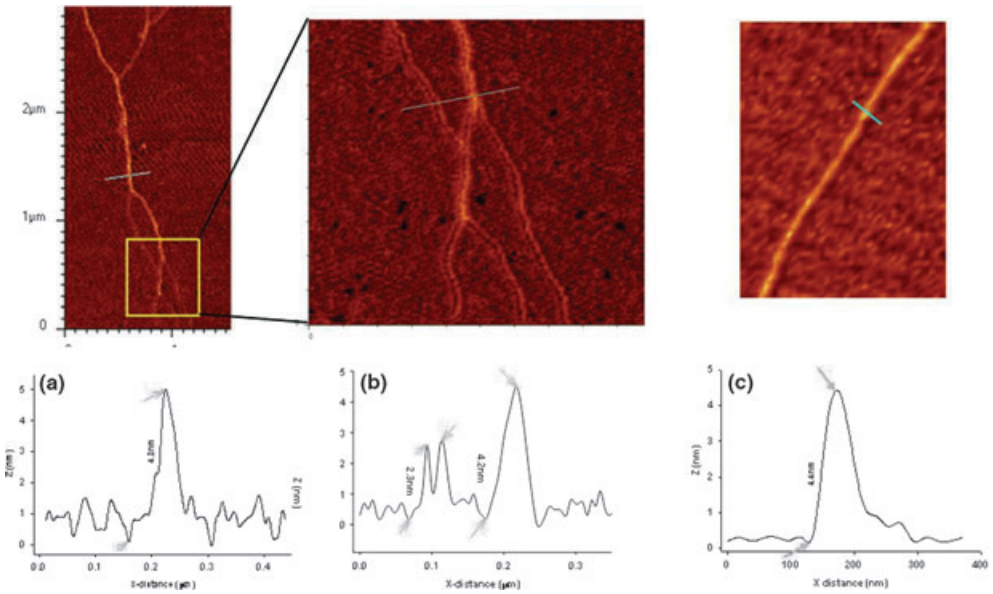

Fig. 4 AFM pictures of oxADan peptides demonstrating various morphological features. All the pictures were extracted from a 3 × 3-mm scan area. The imaging was performed with a scan rate of 0.3 Hz, and the resonance frequency used was 75 kHz. (a) oxADan peptide fibres. The topography along the blue line is shown in the graph below. The height of the fibres is ~4.8 nm. (b) Two sister fibres combine to make one mother fibre. The height of the component fibres (when apart) is ~2.3 nm and after combining it is 4.2 nm (according to the topology along the blue line). (c) Winding of a fibre with itself.

ThT fluorescence, AFM, TEM and Congo red birefringes. Fibrillogenesis in oxADan occurs at only pH 4.9, while in the case of the Aβ peptide it is a spontaneous and rapid process in the pH range 2–8 (Fig. 8a). At pH 2, the Aβ peptide takes only 1 h to mature, followed by 5 h at pH 4.8 and 10 h at pH 8. This, however, is in strong contrast to the case of the ADan peptide, where the fibres take almost 2 weeks to mature at pH 4.8 and fail to mature at all at a higher pH (6–9). As monitored by AFM, the Aβ peptides form fibres of almost the same morphology at all the three pHs presently under consideration (Figs 8a–c). TEM picture of the fibres at pH 4.8 also show well-formed fibres of distinct morphology (Fig. 8d). The amyloidogenic nature of the aggregates was confirmed by the Congo red birefringes obtained under crossed polarized light (Fig. 8e).

Effect of pH and peptide concentration on the fibrillogenesis of ADan peptides

ThT assays were performed on both the reduced and oxidized ADan forms at pH 4.8, 7.0 and 9.0, and at a peptide concentration of 90 μM. This pH range was chosen to keep the experimental parameters proximal to the physiological conditions. Oxidized peptides presented a proper signature of amyloid formation around pH 4.8. A similar conclusion could also be drawn from the far UV–CD spectra of the oxidized peptides at different pHs. On inspecting Fig. 3(b), it is clear that oxADan peptides at pH 4.8 show the initials of β-sheet, while the species at other pHs mostly showed random coil structure. However, none of the far UV–CD spectra obtained for the reduced peptides showed a β-sheet type of conformation, consistent with the fact that ThT assays performed on the redADan also did not show any inscription for fibrillization. Nonetheless, to some extent, an increase in the ThT fluorescence with time was observed for the peptides at pH 4.8, although it was much less compared with that of the oxidized peptides.

Kinetics of fibril formation in ADan peptides

As evident from the ThT fluorescence assays and SDS–PAGE experiments, the fibril formation in the case of ADan peptides is a slow process. In the concentration range 18–140 μM at pH 4.8, the entire process of fibril formation takes almost 10–15 days. A greater scrutiny of the SDS–PAGE picture in Fig. 9 reveals that the oxidized peptide at day 0 (i.e. immediately after starting the reaction) remains mostly as a monomer or a dimer. As the reaction evolves, one finds larger aggregates on days 5 and 12. However, this does not happen for the reduced peptides. Initially, the system consists of a mixture of monomer and dimer. However, with the advancement of the reaction (i.e. on days 10 and 15), the peptides fail to enter the resolving gel. This gives us the impression that the reduced peptides form huge non-specific aggregates that cannot enter the gel (Fig. 9b).

From the size exclusion chromatography experiments carried out on the oxidized form, we find that at the first day (day 0) the system has only the monomeric form, and with the advancement of time aggregates were seen

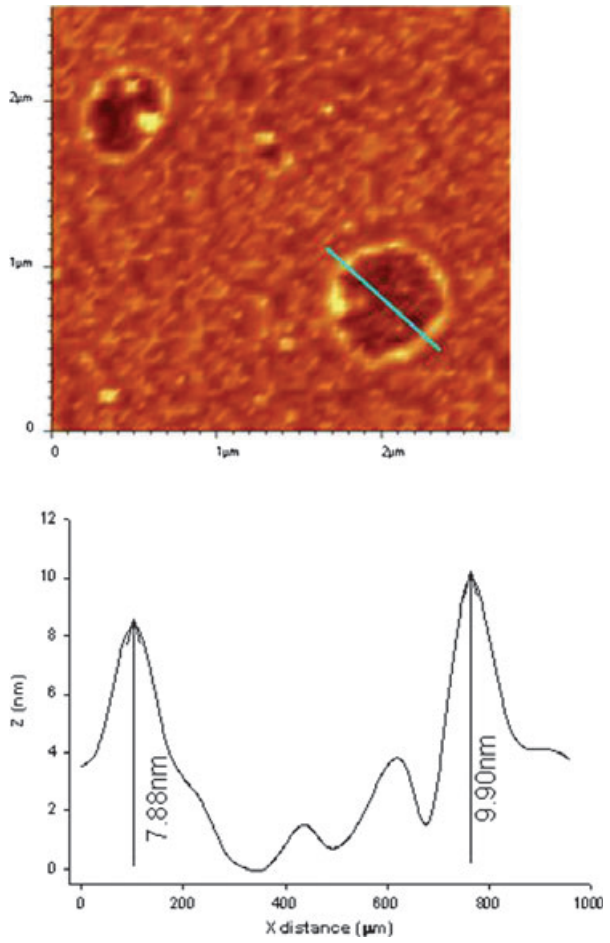

Fig. 5 Annular aggregates obtained from oxADan peptides. The topo logy along the blue line is shown in the graph below. It shows that these aggregates have an average thickness of 8–10 nm.

to occur. At day 5, the monomer peak was depleted by more than 50%, with a consequent rise in the aggregate peak. On day 12, the monomer peak was diminished by more than 80% compared with day 0 and, finally, on day 15 the monomer peak was not seen at all. The inset in Fig. 10 shows the depletion of the monomer (open circles) and the formation of the aggregate (filled circles).

Morphology of the aggregates formed from ADan peptides

The 'make-up' of the fibres formed from the oxADan and redADan peptides were assessed by imaging techniques such as AFM and TEM. The oxidized peptides mostly form long slender structures with a length of several micrometers and a height of 2–5 nm. Occasionally, they form annular bunches of 100 nm diameter. These annular or ring-shaped masses were previously observed with ABri peptides, SMA protein and α-synuclein (Lashuel *et al*. 2002; Srinivasan *et al*. 2004). In the case of α-synuclein, these ring-like aggregates have been suggested to contribute to the pathogenesis of Parkinson's disease (Lashuel *et al*. 2002). For the ABri peptides, the height of the rings is ∼1.5–2.5 nm, while in the case of α-synuclein the height is ∼25–30 nm. In the case of oxADan peptides, however, the height, as determined by AFM, is ∼8–9 nm. Figures 4 and 7(a–d) shows the AFM and TEM pictures, respectively, for the linear fibres obtained from the oxidized peptides. The fibres are fairly straight in morphology. They have very distinct nodes. A careful scrutiny of Fig. 4(a–c) shows that a mature fibre is formed by the entwining of many component fibres. This is better illustrated in the graphs along with the figures. They show the height of the fibres (or basically the topography) along the blue line drawn in the figure. It shows three peaks: two of which are ∼2.3 nm in height and another ∼4.2 nm in height. The first two are the component fibres and the third is a mature fibril filament. The maturation of fibres in oxADan peptides involves the formation of distinct intermediates. Initially, protofibrils are formed followed by immature fibres, which are eventually integrated into adult filamentous forms. Figure 7 shows the chronological sequence for the process of aggregation as monitored by TEM imaging.

The redADan peptides also aggregate to a very well-defined topology. They can be described as 'bell'- or 'dome'-shaped masses with a height of 30–40 nm, as observed in the AFM images. Figure 6 shows the granular aggregates obtained from redADan peptides after incubation of 25 days. The graph alongside shows the topography of the line marked in blue in the figure. It reveals that the aggregates are fairly symmetrical with an average height of 35 nm.

Molecular modelling

Secondary structure prediction of the 34-residue ADan peptide gave two β-strand regions connected by loops. A model of ADan peptide was constructed based on the structure of the 101–123 segment of transthyretin. Residue 1–23 of the ADan peptide was modelled first, considering the structure of the 101–123 segment of transthyretin (PDB (protein data bank) code 1f41) as a template in SwissProt software (http://swissmodel.expasy.org//SWISS-MODEL.html). Later, the residues 23–34 were added to the modelled peptide. The energy of this entire assembly was minimized in Molecular Operating Environment (MOE) software using a force field of AMBER99 (Chemical Computing Group, Inc., Montreal, Quebec, Canada). The final structure achieved is a double-stranded β-sheet connected by a loop; the ends were flanked by a random coil. The two β-strands (spanned by residues 7–11 and 16–21) are held tightly by hydrogen bonds and a disulfide bond between Cys5 and Cys21 residues stabilizes the structure. A β-hairpin turn formed of residues 12–14 joins the two strands. This

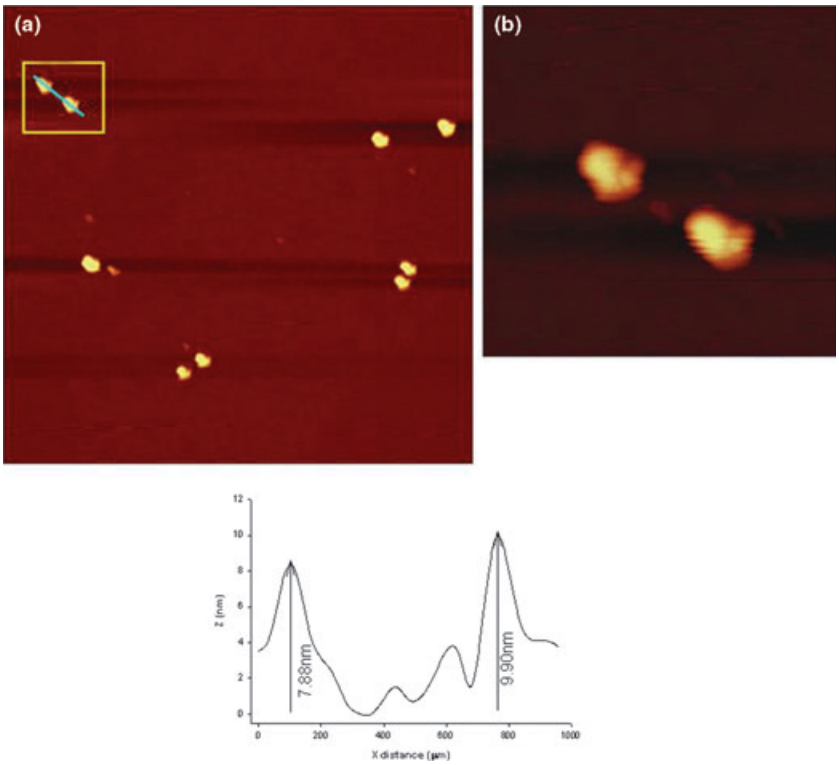

Fig. 6 (a) Morphology of the aggregates formed from the redADan peptides. Dome-shaped assemblies are obtained for the redADan peptides. The topology along the blue line is shown in the graph below. (b) An expanded view of the box in (a).

disulfide bond ties one of the β-strands with the N-terminal loop of the peptide. The modelled monomer is illustrated in Fig. 11(a). The structure of the peptide thus obtained was docked to see the structure of the dimer of the peptide in ClusPro online software (Comeau *et al*. 2004a, 2004b). The docked dimer shows a nice packing of the two monomeric peptides in a parallel array Fig. 11(b). A careful scrutiny of the docked dimer shows that it has an even distribution of hydrogen bonds (Fig. 11). The C-terminal tyrosine residues are also tied to the main β-sheet by hydrogen bonds in both the monomers. It is, however, interesting to note that the monomers do not overlap completely with one another when forming the dimer. Instead, there is a shear in the overlap of the two. Further, hydrophobic groups flank out of the structure, which might be an aid in expanding the structure and finally leading to the formation of the fibres.

Cell neurotoxicity assay

Cell neurotoxicity was assed by treating neuro2a cells with the oxidized and reduced form of the peptides. At lower aggregate concentrations, the reduced peptides are apparently more toxic than the oxidized form. However, at higher

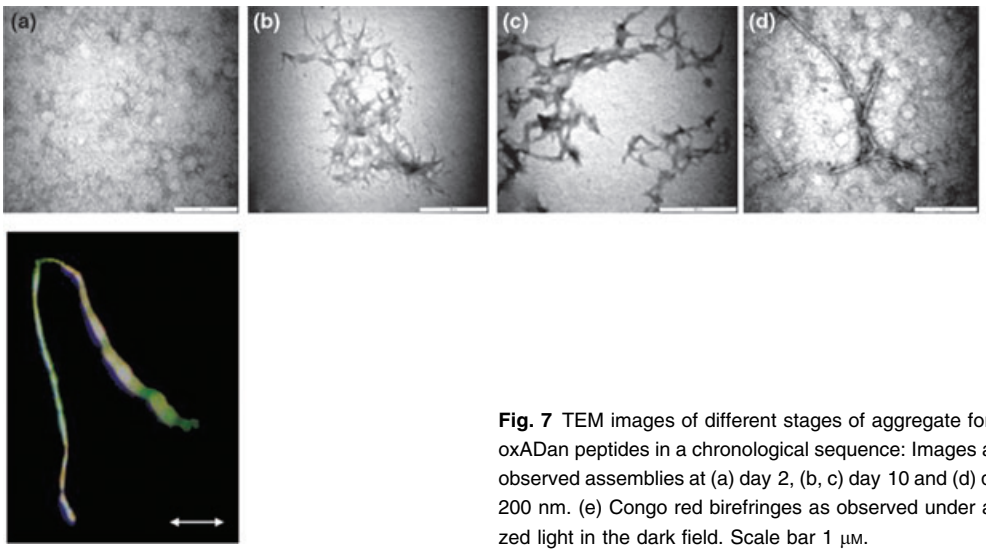

Fig. 7 TEM images of different stages of aggregate formation in the oxADan peptides in a chronological sequence: Images are shown for the observed assemblies at (a) day 2, (b, c) day 10 and (d) day 30. Scale bar 200 nm. (e) Congo red birefringes as observed under a crossed polarized light in the dark field. Scale bar 1 μM.

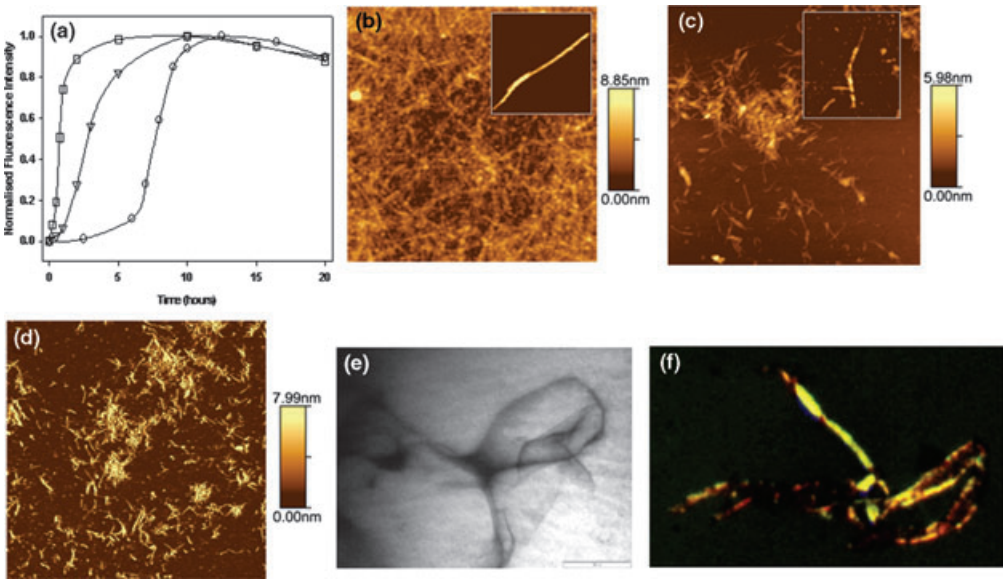

Fig. 8 AFM image of Aβ peptides after incubation for 40 days at different pH values: (a) Kinetics of fibre formation monitored in the case of Aβ peptides at different pH monitored by Thioflavin-T fluorescence (□), pH 2.0 (▽) and pH 4.8 (0) pH 8.0. Morphologies of the Aβ peptides obtained at (b) pH 2.0, (c) pH 4.8 and (d) pH 8. The insets show the zoomed-in view of the single fibres obtained at the respective pHs. The images indicate the beaded nature of the fibrillar assemblies, especially obtained at low pHs, characteristic of the Aβ peptides. (e) TEM image of the Aβ peptide fibre obtained after incubation at pH 4.8 for 1 month. (f) Congo red birefringes obtained from 1-month-old Aβ fibres at pH 4.8.

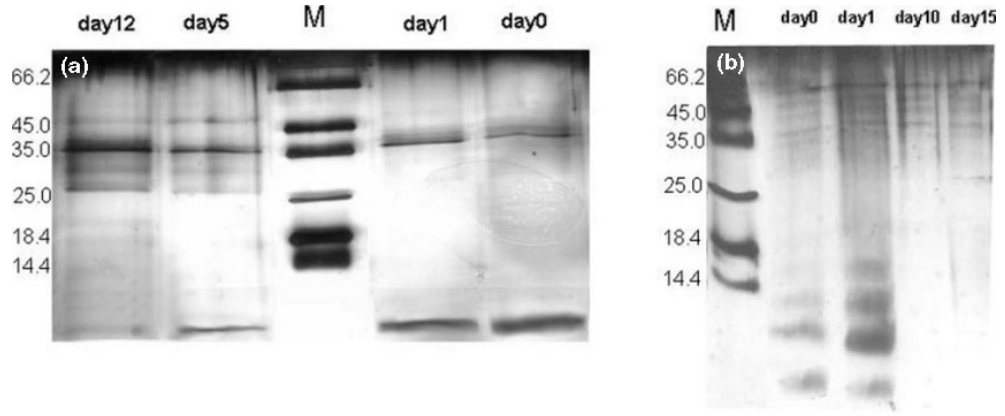

Fig. 9 Fifteen per cent SDS–PAGE of the (a) oxidized and (b) reduced ADan peptides: For the oxidized samples, the samples were frozen from a pool of aggregating peptides on days 0, 1, 5 and 12, while for the reduced ones the samples were frozen on days 0, 1, 10 and 15.

concentrations, the effect of both seems to be the same. At a concentration of ∼150 μM, both forms of the peptides are toxic to the same extent, as assayed by MTT and trypan blue exclusion assay (Fig. 12).

Discussion

Fibrillogenesis can be described as the transformation of the natively unfolded polypeptide to a β-sheet-rich polymer. All the experiments designed in this study attempt to delineate the effect of pH and peptide concentration on the mechanism of fibril formation by ADan peptides in the oxidized and reduced forms. We also attempt to deal with the morphological characterization of these assemblies under different conditions and to compare the nature of the fibres obtained here with the amyloidogenic peptides such as Aβ peptide.

The experiments documented here equivocally indicate that the oxADan peptides form long slender fibrillar assemblies, while the reduced ones associate to produce globular aggregates only at pH 4.9. The theoretical pI of the peptide,

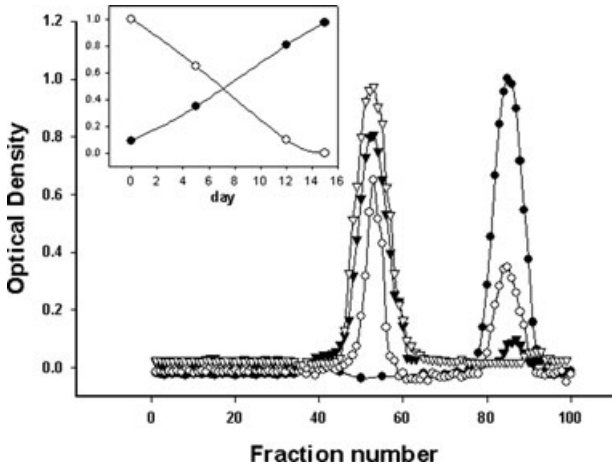

Fig. 10 Gel filtration profile of the oxADan peptides; oxADan peptides show the gradual formation of aggregates and the depletion of the monomer with time. Day 0 (●), day 5 (○), day 12 (▼) and day 15 (▽). The inset shows the depletion of the monomer (○) and the formation of the aggregate (●) with time.

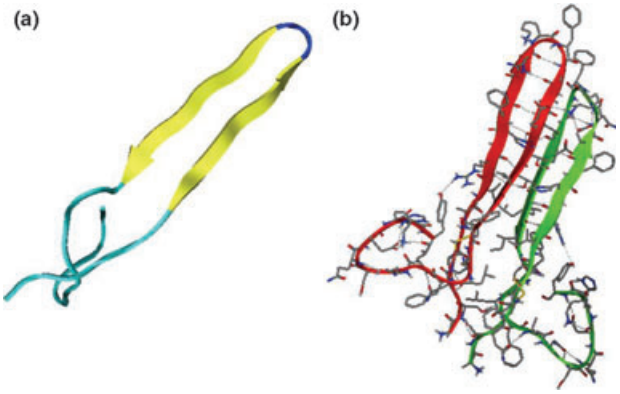

Fig. 11 (a) The monomer of the oxADan peptide modelled using SwissProt software: The yellow portions are the two β-sheets joined by a dark blue β-turn. The light blue portions are random coils. (b) The dimer of the peptide docked in ClusPro online software (Comeau *et al.* 2004a,b).

as calculated from protparam, is 6.9. Hence, it is not simple to solubilize the peptides at near physiological pH. The peptides will have a tendency to salt out as amorphous aggregates rather than forming the fibrils at higher pHs. The disulfide bond in the oxidized species imparts to the peptide the requisite topology for the formation of the β-sheet array, while, in the reduced one, the free cysteins possibly combine to form huge non-specific aggregates. Figure 2(c) shows the ThT assay monitored with both the forms under identical conditions. In both cases, there is enhancement of the ThT fluorescence signal, the enhancement being more in the case of the oxADan peptides. It may be because both the forms initially start forming fibrillar assemblies. However, eventually the oxidized peptides lead to the formation of mature

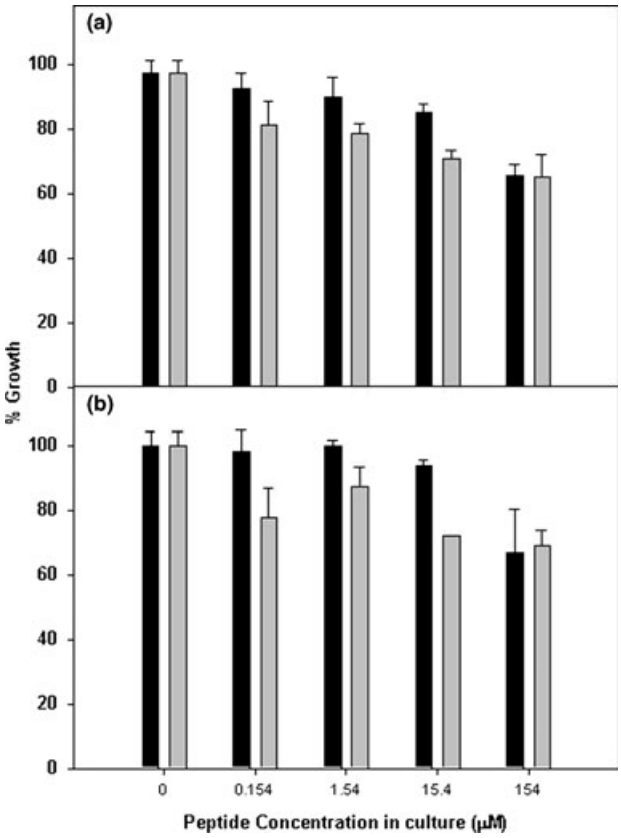

Fig. 12 Cell neurotoxicity assay performed on neuro2a cells: Neurotoxicity was monitored by (a) Trypan blue exclusion and (b) MTT uptake by the cells. Percentage of growth is recorded on the *y*-axis.

fibres and the reduced ones do not. The assays were performed on the oxidized peptides in the concentration range 18–140 μM. For each of the assays, a well-defined sigmoid curve was obtained which suggests the inherent cooperativity of the process of fibrillogenesis. After reaching its maxima, the ThT fluorescence drops down for all concentrations. This is because, in time, amorphous aggregates also start crowding the system.

In general, the rates of formation of the amorphous moieties are higher than the rates of formation of the amyloid species. Thus, there exists a competition between the kinetically controlled and the thermodynamically controlled products which leads to the fall in ThT fluorescence. Surprisingly, it was also discovered that increasing the concentration of the peptide resulted in the decrease in the rate of fibril formation. In other words, there is a 'lag phase' in the process of fibre maturity as one goes on increasing the concentration of the peptide solution. A closer look into Fig. 1(a) illustrates this explicitly. The increase in the lag phase over time indicates that there must be a stable monomeric intermediate which dictates the initiation of the event of aggregation. At higher concentrations, the rate of formation of the monomer is accordingly expected to be

slow. Hence, there is a delay in the process of fibrillization at higher concentrations. This is in agreement with the mechanism of fibril formation in Aβ (25–35) which also underscores the stability of the monomeric intermediate in regulating its ability to form fibrils (Ma and Nussinov 2006). Also, it has been reported that β-2-microglobulin also aggregate via a native-like folding intermediate (Jahn *et al*. 2006). In spite of this, the actual amount of fibres formed is directly proportional to the initial concentration of the peptides used in the reaction. This is shown in Fig. 1(c), where the maximum ThT fluorescence is plotted against concentration. The plot is a linear one with a positive slope, indicating that the amount of fibres formed is a function of the concentration of the peptides used. According to Srinivasan *et al*. (2003), in ABri peptides the rate of fibre formation increases with an increase in the concentration of the peptides. In the experiments carried out with 56 μM ABri peptides, there is a lag phase of only 6 h. In our experiments with ADan concentrations of 35, 70, 100 and 140 μM, the lag phases are, respectively, 22, 58, 97 and 94 h. Thus, the mechanism of fibril formation is not exactly identical in the ABri and ADan peptides, although the mature fibres in either case are morphologically similar. Fully mature ADan aggregates result from entwining of two newly formed fibres laterally; thus two individual sister components form the mother fibre (Fig. 4b). A closer examination of Fig. 4(c) shows the entwining of a single mature fibre with itself. For the ABri peptides, the authors propose that the mature fibres are formed from the assembly of smaller aggregates in a linear fashion (as observed by the periodicity in the morphology of the ABri fibres). No periodicity is, however, observed for oxADan peptides. Further, in none of the images (AFM or TEM), small globular aggregates similar to the one found in the case of ABri peptides are obtained. The morphology of fibres obtained of the Aβ peptides (which are considered to be a key cause in the pathogenesis of Alzheimer's disease) is quite a contrast from those of the oxADan peptides. The manifestation of the Aβ peptide fibres as envisaged from AFM and TEM imaging are shown in Fig. 8. A closer assessment of Figs 8(a–c) indicates that the topology of the fibres derived from ADan and Aβ peptides are quite different. The beaded appearance in the case of Aβ peptides (especially at lower pHs), in contrast to the entwined appearance in the case of ADan peptides, clearly implies the difference in their mode of aggregation. The aggregates in the case of the former are made up of small globules adhering together, while, in the case of the latter, the plaques are a result of entwining of sister threads. During the course of AFM measurements of the Aβ peptides, we have come across many small globular particles with dimensions of ~3–5 nm. Probably these globular masses club together and form the fibrillar aggregates. This mechanism of fibril formation has previously been proposed by many amyloidogenic peptides/proteins. Nonetheless, in the case of ADan peptides, we have not come across such globular entities in AFM studies. However, the mature fibres in either case are of the similar dimensions. For example, the Aβ peptides produce mature fibres which are nearly 5 nm in diameter (as obtained from histogram analyses) and span almost a length of a few hundred nanometers. Thus, it is seen that, although there are differences in the maturation of the two peptides, the final dimensions of the fibres are the same and hence may have similar implications in the pathogenesis of the disease. Further, the process of fibrillogenesis in the Aβ peptides is quite fast when compared with the ADan peptides. Although, in Aβ peptides, the kinetics of aggregation is pH dependent, the process is much faster compared with the case of ADan peptides. The process is fastest at pH 2 and is completed in 1 h. At pH 4.8 and 8 the peptides take 2 and 6 h, respectively, to form fibril assemblies.

Fluorescence polarization studies performed on the oxADan peptides imply that the environment of the C-terminal tyrosine residue experiences diminished mobility upon fibrilization. These experiments were carried out with the centrifuged and non-centrifuged sample solutions (see Materials and methods). Figure 13 shows the pattern of anisotropy obtained for the respective samples over time. In the centrifuged samples, there was an initial increase in the polarization values followed by a gradual drop. At the initial phases, the aggregates formed are smaller in size and hence cannot be precipitated out by centrifugation. These soluble aggregates hinder the movement of the C-terminal tyrosine residue and consequently an increase in the polarization. However, with the advancement of the reaction, the fibrillar assemblies grow bigger and can be easily separated by centrifugation. Similarly, one can anticipate the sequence of events in the non-centrifuged vials. Although sluggish, from

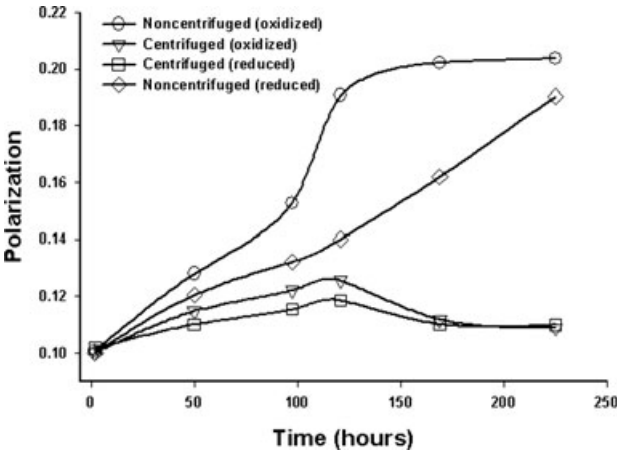

Fig. 13 Fluorescence polarization experiments performed on the oxADan and redADan peptides: Polarization was recorded for the C-terminal tyrosine in the peptides. Samples were excited at 280 nm and the polarization was measured at 305 nm according to the equation (see Materials and methods).

the beginning there is an increase in the polarization in these samples. After a gradual increase in the polarization value (until 100 h) there is a sudden sharp increase. After 120 h, the polarization value stabilizes, indicating that the process is complete and the peptides have bundled together to form fibres of fixed size. Hence, one can infer that the process of fibril formation starts as soon as the peptides are dissolved in the buffer. The small increase in the polarization in this phase is an indication of the formation of small protofibrillar aggregates, and the greater rise in the polarization later in the process indicates the formation of mature fibres. If we compare the two profiles, we see that the fall in the polarization value for the centrifuged vial occurs at the same time, when there was a steep increase in the same for the non-centrifuged samples. Similar inferences about the kinetics are obtained from the ThT assays. The behaviour of the reduced peptides, however, is slightly different. For the centrifuged samples, the observations are similar; but the scenario changes as one sees the non-centrifuged vials; from the very beginning there is a gradual increase in the polarization. This indicates that the process of aggregation initiates from the start and the aggregates formed are not of finite size, as observed in the case of the oxidized samples.

Toxicity studies demonstrate that, at lower concentrations of the peptides, the reduced one is more toxic as compared with its oxidized counterpart, while at higher concentrations the toxicity of both of them are similar. The reduced form of the peptide has an inherent tendency to form large aggregates and, as these aggregates are non-specific, they start accumulating from the very beginning when the peptide concentration is much less. However, this is not the case with the oxidized form. These peptides have a definite relationship to growth which shows a correlation with their concentration in solution. Thus, our results correlate the toxicity of the peptides with the size of the aggregates formed and not with their morphology. As the size of the aggregating component increases, its multivalency increases, giving rise to an increase in the toxicity. At very low concentrations of 154 nM of the peptides, the reduced one shows a decrease in ~20% cell growth, while there is negligible effect in the cell with the oxidized peptides (Fig. 12). Only at a peptide concentration of 15.4 μM does the oxidized form shows a ~6–8% loss in cell growth. At this concentration, the reduced peptides show a ~30–35% loss in the growth. However, at a 154-μM concentration, both forms show equal loss in cell development, proving that it is not the form of the peptide but the mass of the aggregate which causes cell death.

Conclusions

There are several interesting outcomes of the present study. Firstly, for example, we also establish that the oxADan form stable fibres at pH 4.8. The reduced form is unable to produce fibres at any of the conditions in the range of pH 4.8–9. Next, it is obvious from our studies that the disulfide bond plays an intricate role in the fate of the fibres in the case of ADan peptides. Also, another morphological variant of the aggregates, the ring or the annular type, has also been reported. Last, but not least, we have shown that it is the size of the aggregate that controls cell death rather than the shape or the form. Hence, therapeutic strategies which can arrest the process of fibrillogenesis at an early stage should be designed to fight the diseases resulting from the aggregation deposits.

Acknowledgements

The authors thank the Chairman of MBU, IISc for extending the facilities of his laboratory and his constant encouragement in pursuing the work. We also thank Professor D. Panda (IIT, Mumbai, India) for allowing the use of the TEM facility. Furthermore, we thank Dr Shashi Singh (CCMB, Hyderabad, India) and Dr G. Sivashankar (NCBS, Bangalore, India) for access to their AFM. We thank Dr R. Manjunath (Department of Biochemistry, IISc, India) for the neuro2a cells and Dr D. P. Sarkar, Department of Biochemistry, University of Delhi, India for insightful discussions. SS thanks the Council for Scientific and Industrial Research, India for the award of Senior Research Fellowship and IS thanks ICMR for the award of a Research fellowship.

References

Agorogiannis E. I., Agorogiannis G. I., Papadimitriou A. and Hadjigeorgiou G. M. (2004) Protein misfolding in neurodegenerative diseases. *Neuropathol. Appl. Neurobiol.* **30**, 215–224.

Comeau S. R., Gatchell D. W., Vajda S. and Camacho C. J. (2004a) ClusPro: an automated docking and discrimination method for the prediction of protein complexes. *Bioinformatics* **20**, 45–50.

Comeau S. R., Gatchell D. W., Vajda S. and Camacho C. J. (2004b) ClusPro: a fully automated algorithm for protein–protein docking. *Nucleic Acids Res.* **32**, W96–W99,.

Das A. K., Drew M. G. B., Haldar D. *et al.* (2005) The role of disulphide bond in amyloid-like fibrillogenesis in a model peptide system. *Org. Biomol. Chem.* **3**, 3502–3507.

Dobson C. M. (1999) Protein misfolding, evolution and disease. *Trends Biochem. Sci.* **24**, 329–332.

Foguel D. and Silva J. L. (2004) New insights into the mechanisms of protein misfolding and aggregation in amyloidogenic diseases derived from pressure studies. *Biochemistry* **43**, 11 361–11 370.

Gibson G., Gunasekera N. and Lee M. (2004) Oligomerization and neurotoxicity of the amyloid ADan peptide implicated in familial Danish dementia. *J. Neurochem.* **88**, 281–290.

Horwich A. L. and Weissman J. S. (1997) Deadly conformations – protein misfolding in prion disease. *Cell* **89**, 499–510.

Ionescu-Zanetti C., Khurana R., Gillespie J. R., Petrick J. S., Trabachino L. C., Minert L. J., Carter S. A. and Fink A. L. (1999) Monitoring the assembly of Ig light-chain amyloid fibrils by atomic force microscopy. *Proc. Natl Acad. Sci. USA* **96**, 13 175–13 179.

Jahn T. R., Parker M. J., Homans S. W. and Radford S. E. (2006) Amyloid formation under physiological conditions proceeds via a native-like folding intermediate. *Nat. Struc. Mol. Biol.* **13**(3), 195–201.

Krebs M. R. H., Bromley E. H. C. and Donald A. M. (2004) The binding of thioflavin-T to amyloid fibrils: localisation and implications. *J. Struct. Biol.* **149**, 30–37.

Laemmli U. K. (1970) Cleavage of structural proteins during the assembly of the head of bacteriaphage T4. *Nature* **227**, 680–685.

Lashuel H. A., Petre B. M., Wall J., Simon M., Nowak R. J., Walz T. and Lansbury P. T. Jr (2002) α-Synuclein, especially the Parkinson's disease-associated mutants, forms pore-like annular and tubular protofibrils. *J. Mol. Biol.* **322**, 1089–1102.

Ma B. and Nussinov R. (2002) Molecular dynamics simulations of alanine-rich β-sheet oligomers: insight into amyloid formation. *Protein Sci.* **11**, 2335–2350.

Ma B. and Nussinov R. (2006) The stability of monomeric intermediates controls amyloid formation: Aβ25-35 and its N27Q mutant. *Biophys. J.* **90**(10), 3365–3374.

Mitra N., Sinha S., Ramya T. N. and Surolia A. (2006) *N*-linked oligosaccharides as outfitters for glycoprotein folding, form and function. *Trends Biochem. Sci.* **31**, 156–163.

Nelson R., Sawaya S. R., Balbirnie M. *et al.* (2005) Structure of the cross-b spine of amyloid-like fibrils. *Nature* **435**, 773–778.

Nielsen L., Frokjaer S., Brange J., Uversky V. N. and Fink A. L. (2001) Probing the mechanism of insulin fibril formation with insulin mutants. *Biochemistry* **40**(28), 8397–8409.

Phillips H. J. (1973) Dye exclusion tests for cell viability, in *Tissue Culture: Methods and Applications* (Kruse P. F. Jr and Patterson M. K.Jr , eds), pp. 406–408. Academic Press Inc., New York.

Pras M., Schubert M., Zucker-Franklin D. *et al.* (1968) The characterization of soluble amyloid prepared in water. *J. Clin. Invest.* **47**, 924–933.

Ramos C. H. and Ferreira S. T. (2005) Protein folding, misfolding and aggregation: evolving concepts and conformational diseases. *Protein Pept Lett.* **12**, 213–222.

Recchia A., Debetto P., Negro A., Guidolin D., Skaper S. D. and Giusti P. (2004) α-Synuclein and Parkinson's disease. *FASEB J.* **18**, 617–626.

Ross C. A. and Pickart C. M. (2004) The ubiquitin–proteasome pathway in Parkinson's disease and other neurodegenerative diseases. *Trends Cell Biol.* **14**, 703–711.

Ruben G. C., Iqbal K., Wisniewski H. M., Johnson J. E. Jr and Grundke-Iqbal I. (1993) Alzheimer neurofibrillary tangles contain 2.1 nm filaments structurally identical to the microtubule-associated protein tau: a high-resolution transmission electron microscope study of tangles and senile plaque core amyloid. *Brain Res.* **602**, 164–179.

Selkoe D. J. (2004) Cell biology of protein misfolding: the examples of Alzheimer's and Parkinson's diseases. *Nat. Cell Biol.* **6**, 1054–1061.

Sikorski P. and Atkins E. (2005) New model for crystalline polyglutamine assemblies and their connection with amyloid fibrils. *Biomacromolecules* **6**, 425–432.

Soto C. (2003) Unfolding the role of protein misfolding in neurodegenerative diseases. *Nat. Rev. Neurosci.* **4**, 49–60.

Srinivasan R., Jones E. M., Liu K. *et al.* (2003) pH-dependent amyloid and protofibril formation by the ABri peptide of familial British dementia. *J. Mol. Biol.* **333**, 1003–1023.

Srinivasan R., Marchant R. E. and Zagorski M. G. (2004) ABri peptide associated with familial British dementia forms annular and ring-like protofibrillar structures. *Amyloid* **11**, 10–13.

Stine W. B. Jr, Dahlgren K. N. and Krafft G. A. (2003) *In vitro* characterization of conditions for amyloid-β peptide oligomerization and fibrillogenesis. *J. Biol. Chem.* **278**, 11 612–11 622.

Thompson A. J. and Barrow C. J. (2002) Protein conformational misfolding and amyloid formation: characteristics of a new class of disorders that include Alzheimer's and Prion diseases. *Curr. Med. Chem.* **9**, 1751–1762.

Vidal R., Revesz T., Rostagno A., Kim E. *et al.* (2000) A decamer duplication in the 3′ region of the BRI gene originates an amyloid peptide that is associated with dementia in a Danish kindred. *Proc. Natl Acad. Sci. USA* **97**, 4920–4925.

Westermark P. (2005) Aspects of human amyloid forms and their fibril polypeptides. *FEBS J.* **272**, 5971–5978.

Zanuy D., Ma B. and Nussinov R. (2003) Short peptide amyloid organization: stabilities and conformations of the islet amyloid peptide NFGAIL. *Biophys. J.* **84**, 1884–1894.

